Sequential Bond Energies of $Fe^+(CO_2)_n$, $n = 1-5$, Determined by Threshold Collision-Induced Dissociation and ab Initio Theory†

P. B. Armentrout,* Hideya Koizumi, and Meghan MacKenna‡

Department of Chemistry, University of Utah, Salt Lake City, Utah 84112

Received: May 4, 2005; In Final Form: June 23, 2005

Collision-induced dissociation of the $Fe^+(CO_2)_n$ complexes for $n = 1-5$ is studied using kinetic energy dependent guided ion beam mass spectrometry. In all cases, the primary products are endothermic loss of an intact neutral ligand from the complex. The cross section thresholds are interpreted to yield 0 K bond energies after accounting for the effects of multiple ion−molecule collisions, internal energy of the complexes, and unimolecular decay rates. These values are compared with density functional theoretical values for all five complexes. Theory provides bond energies in reasonable agreement with experiment for $n = 1-4$ and predictions for the infrared spectroscopy of these complexes that agree nicely with experimental results of Gregoire and Duncan (*J. Chem. Phys.* **2002**, *117*, 2120). Our thermochemical results are also compared with the $Fe^+(CO)_n$ and $Fe^+(N_2)_n$ complexes, previously studied.

1. Introduction

The possibility of using abundant carbon dioxide (CO_2) as a starting material for synthesis of chemically useful compounds has received considerable attention.[1−5] To better understand the role of metals in the catalytic utilization of CO_2, a useful starting point may be gas-phase studies. Several studies have focused on the experimental[6−8] and theoretical[9,10] characterization of the $Fe^+(CO_2)$ complex, including its bond energy. This was determined to be 0.56 ± 0.08 eV by Schwarz and co-workers,[7] a value later refined to 0.63 ± 0.08 eV, which agrees well with a value of 0.62 ± 0.04 eV obtained using collision-induced dissociation (CID) studies performed in our laboratories.[8] Recently, Gregoire and Duncan have studied $Fe^+(CO_2)_n$ and $Fe^+(CO_2)_nAr$ clusters by infrared photodissociation spectroscopy.[11] In their studies, all small complexes ($n \leq 6$) have resonances shifted to higher frequencies than the asymmetric stretch of free CO_2 molecules. These bands were attributed to the core ligands attached directly to the metal center. For larger clusters ($n \geq 4$), they observed resonances near the free CO_2 asymmetric stretch frequency, which they suggest indicate parallel structures, "T" shaped structures, or CO_2 ligands that are not bound directly to the Fe^+ ion. Their study also provides qualitative information that the $Fe^+(CO_2)_2$ complex is particularly stable; however, no quantitative bond dissociation energies (BDEs) can be measured using this technique.

In recent years, complexes of transition-metal cations M^+ with multiple ligands have been studied extensively to understand metal ligand interactions and the solvation process. Because of the open shell character of most transition metals, the sequential metal ligand BDEs do not necessarily decrease monotonically as n increases. This behavior cannot be rationalized on the basis of increasing steric effects or decreasing effective charge at the metal center. A good example of such trends in sequential BDEs is observed for iron cation complexes. Previously, our lab studied CID of $Fe^+(CO)_n$ and $Fe^+(N_2)_n$ for $n = 1-5$, and $Fe^+(CH_2O)_m$, $Fe^+(H_2O)_m$, and $Fe^+(NH_3)_m$ for $m = 1-4$.[12−15] Bushnell, Kemper, and Bowers studied $Fe^+(H_2)_n$ for $n = 1-6$ via temperature-dependent equilibrium measurements.[16] In all cases, the strongest BDE is found for the second ligand. Also, a relatively strong fourth BDE is observed for π-accepting ligands (N_2, CO, and H_2), whereas a relatively weak fourth BDE is observed for π-donating ligands (CH_2O and H_2O). The rationale for these trends has been discussed[17] and is explored further in the discussion below.

In this project, we investigate the binding of Fe^+ to $1-5$ CO_2 molecules. Guided ion beam mass spectrometry is used to measure the kinetic energy dependent cross sections for CID of these complexes with Xe. Analysis of these results provides absolute binding energies of these complexes after consideration of reactant energy distributions, effects of multiple collisions, and lifetime effects. These results are compared to density functional theoretical (DFT) results on all five complexes and to previous theoretical work on $Fe^+(CO_2)$.[9,10] The trend in the sequential BDEs for CO_2 is compared with those previously measured for other iron complexes.[12−16]

2. Experimental and Theoretical Methods

2.1. Experimental Approach. For all reactions studied here, cross sections are collected using a guided ion beam tandem mass spectrometer (GIBMS) described previously.[18−20] $Fe^+(CO_2)_n$ complexes are produced at the front end of a meter long flow tube, where a dc discharge in a ~10% mixture of Ar in He creates Ar^+ ions that sputter metal ions from an iron cathode. The overall pressure is about 0.5 Torr and typical operating conditions of the dc discharge are 2.7 kV and 20 mA. CO_2 molecules are introduced about 50 cm downstream of the source and attached to the Fe^+ ions by three-body condensation. While the complexes traverse the remainder of the flow tube, they are thermalized by undergoing $>10^4$ collisions with the bath gases. The assumption of efficient thermalization is reasonable, as suggested by previous work.[12,21−24] Under typi-

† Part of the special issue "Jack Simons Festschrift". Congratulations and thanks to a great friend and colleague.

‡ R.E.U. student.

10.1021/jp052317x CCC: $30.25
Published on Web 08/13/2005

cal flow tube conditions, the intensities of the reactant ion beams are $(2-5) \times 10^4$ s^{-1} for the $Fe^+(CO_2)$ and $Fe^+(CO_2)_2$ complexes and very small for $Fe^+(CO_2)_3$ ($<10^4$ s^{-1}). Larger intensities ($\sim 10^5$ s^{-1}) are observed for $Fe^+(CO_2)_4$ and $Fe^+(CO_2)_5$.

These ions are extracted from the source, accelerated, and focused into a magnetic sector momentum analyzer for mass analysis. The mass-selected ions are slowed to a desired kinetic energy and focused into an rf octopole ion guide.[18,20,25] The guide passes through a static gas cell containing xenon gas, used in our CID studies for reasons described elsewhere.[21,26] After exiting the gas cell, the product and remaining reactant ions drift to the end of the octopole, where they are extracted and focused into a quadrupole mass filter for mass analysis. A secondary electron scintillation ion counter detects the mass-analyzed reactant and product ions. These signals are converted to absolute reaction cross sections as described previously.[18] Absolute uncertainties in these cross sections are estimated to be ±20%.

Sharp features in observed cross sections are broadened by thermal motion of the xenon gas and the distribution of ion energies. The distribution and absolute zero of the ion kinetic energies are measured using the octopole as a retarding potential analyzer.[18] The uncertainty in the absolute energy scale is ±0.05 eV (lab). Typical distributions are Gaussian with a full width at half-maximum (fwhm) between 0.2 and 0.5 eV (lab). Kinetic energies in the laboratory frame are converted to ion energies in the center-of-mass (CM) frame by $E(\mathrm{CM}) = E(\mathrm{lab})m/(M + m)$, where M and m are ion and neutral reactant masses, respectively. All energies cited in this paper are in the CM frame except as noted.

2.2. Theoretical Approach. The ground state of Fe^+ is $^6D(4s^13d^6)$, with an excited $^4F(3d^7)$ state lying 0.25 eV higher in energy (energies are the statistical average over the spin−orbit levels).[27] Accurate electronic energies of the bare Fe^+ ion are inaccurately calculated using standard density functional approaches (B3LYP, B3P86, etc.) because these calculations tend to overestimate the stability of the d^{n+1} configurations with respect to s^1d^n. This may become problematic when calculating the BDEs for Fe^+ ion complexes. Sodupe et al.[9] calculated the ground state of Fe^+ ion using B3LYP with a small basis set, [8s4p3d] contraction of the (14s9p5d) primitive set of Wachters[28] supplemented with two diffuse p and one diffuse d functions.[29] They found a quartet ground state (^4F) at this level, 0.16 eV lower than the sextet state, whereas their CCSD(T) calculations using averaged atomic natural orbital (ANO) basis sets[30] correctly predicted the ground state of Fe^+ ion as a sextet (^6D), 0.20 eV lower than the quartet state. Accurate ab initio calculations at the CCSD(T) level become expensive for $Fe^+(CO_2)_n$ ion complexes with n larger than 2. Indeed, we are unaware of any previous calculations on $Fe^+(CO_2)_n$ complexes larger than $n = 2$. Interestingly, the BHandH functional with a 6-311+G* basis set predicts that the ground state of Fe^+ is sextet with an excitation energy to the lowest excited quartet of 0.30 eV, compared to the experimental value of 0.25 eV. Therefore, calculations on all $Fe^+(CO_2)_n$ complexes are performed at the BHandH/6-311+G* level of theory using the Gaussian98W suite of programs.[31] This level was used for all geometry and frequency calculations, which verified that the geometries found correspond to stable minima on the potential energy surface. The energies of all species were also calculated at this level and corrected for zero point energies. The vibrational frequencies were scaled by factors of 0.926 on the basis of the average factor needed to correct the frequencies calculated for CO_2 to match the experimental values.[32] No basis set superposition error (BSSE) corrections were applied in this work, in large measure because we have found such corrections to be quite small (<0.02 eV) for density functional calculations and because the accuracy of the theoretical bond energies is not sufficiently high that such minor corrections make an appreciable difference in the comparison with experiment. For comparison purposes, single point energies for several species were also calculated at the CCSD(T)/6-311+G* ($n = 1$ and 2) level using the BHandH optimized geometries and also at the B3LYP/6-311+G*//B3LYP/6-311+G* ($n = 1-4$) level. The CCSD(T)/6-311+G*//BHandH/6-311+G* level predicts a sextet ground state for Fe^+ by 0.336 eV, in reasonable agreement with experiment, whereas the B3LYP/6-311+G* level obtains a quartet ground state lying 0.205 eV below the sextet. In the following, the BHandH/6-311+G*//BHandH/6-311+G*, B3LYP/6-311+G*//B3LYP/6-311+G*, and CCSD(T)/6-311+G*//BHandH/6-311+G* calculations will be referred to simply as BHandH, B3LYP, and CCSD(T).

3. Results

3.1. Experimental Observations. Experimental cross sections for the collision-induced dissociation (CID) of $Fe^+(CO_2)_n$, $n = 1-5$, complexes with xenon are shown in Figure 1. The primary process for all complexes is the loss of a single CO_2 ligand in reaction 1.

$$Fe^+(CO_2)_n + Xe \rightarrow Fe^+(CO_2)_{n-1} + CO_2 + Xe \qquad (1)$$

For $n = 1$, the cross sections for this reaction are basically identical to results published previously,[8] and shown here for comparison with the larger complexes. Briefly, the Fe^+ ion product cross section has an apparent threshold of about 0.5 eV and increases to a maximum magnitude of about 12 Å^2 at 3 eV. The Fe^+Xe ligand exchange product ion is also observed for this reaction. Its cross section is essentially flat below 0.3 eV before declining as $E^{-1/2}$ from 0.3 to 0.6 eV and more sharply above 0.6 eV. The low energy behavior is consistent with a slightly endothermic reaction, as previously characterized in detail.[8] The sharp decrease at higher energies is caused by the decomposition of the product to form Fe^+ and Xe.

For $n = 2$, the $Fe^+(CO_2)$ ion product cross section has an apparent threshold near 0.6 eV and levels off with a maximum magnitude of 25 Å^2 (about twice the magnitude of the $Fe^+(CO_2)$ CID cross section). The $Fe^+(CO_2)Xe$ ligand exchange product has an apparent threshold near 0 eV and a maximum magnitude of 4 Å^2 at 0.8 eV. This cross section decreases at energies above the onset for the $Fe^+(CO_2)$ indicating that the product decomposes by losing Xe. A small amount of the secondary product Fe^+ ion was observed in this reaction. It has an apparent threshold near 1.8 eV and slowly increases to its maximum magnitude of 2.5 Å^2 at 4 eV.

For $n = 3$, the $Fe^+(CO_2)_2$ primary product ion cross section has an finite cross section at 0 eV and increases rapidly to its maximum magnitude of 70 Å^2 by 1 eV. A small amount of the secondary $Fe^+(CO_2)$ product ion was also observed. Its cross section has an apparent threshold near 1.0 eV and slowly increases to a magnitude of 14 Å^2 at 4 eV. No Fe^+ ion or ligand exchange products (e.g., $Fe^+(CO_2)_2Xe$) are observed at all energies studied. For $n = 4$, the $Fe^+(CO_2)_3$ cross section has an apparent threshold of 0.2 eV and reaches a maximum of 50 Å^2 at 2 eV. The secondary $Fe^+(CO_2)_2$ product ion has a cross section with an apparent threshold of about 1.5 eV and increases steadily over the energy range studied. For $n = 5$, the cross section for the primary product $Fe^+(CO_2)_4$ has an apparent

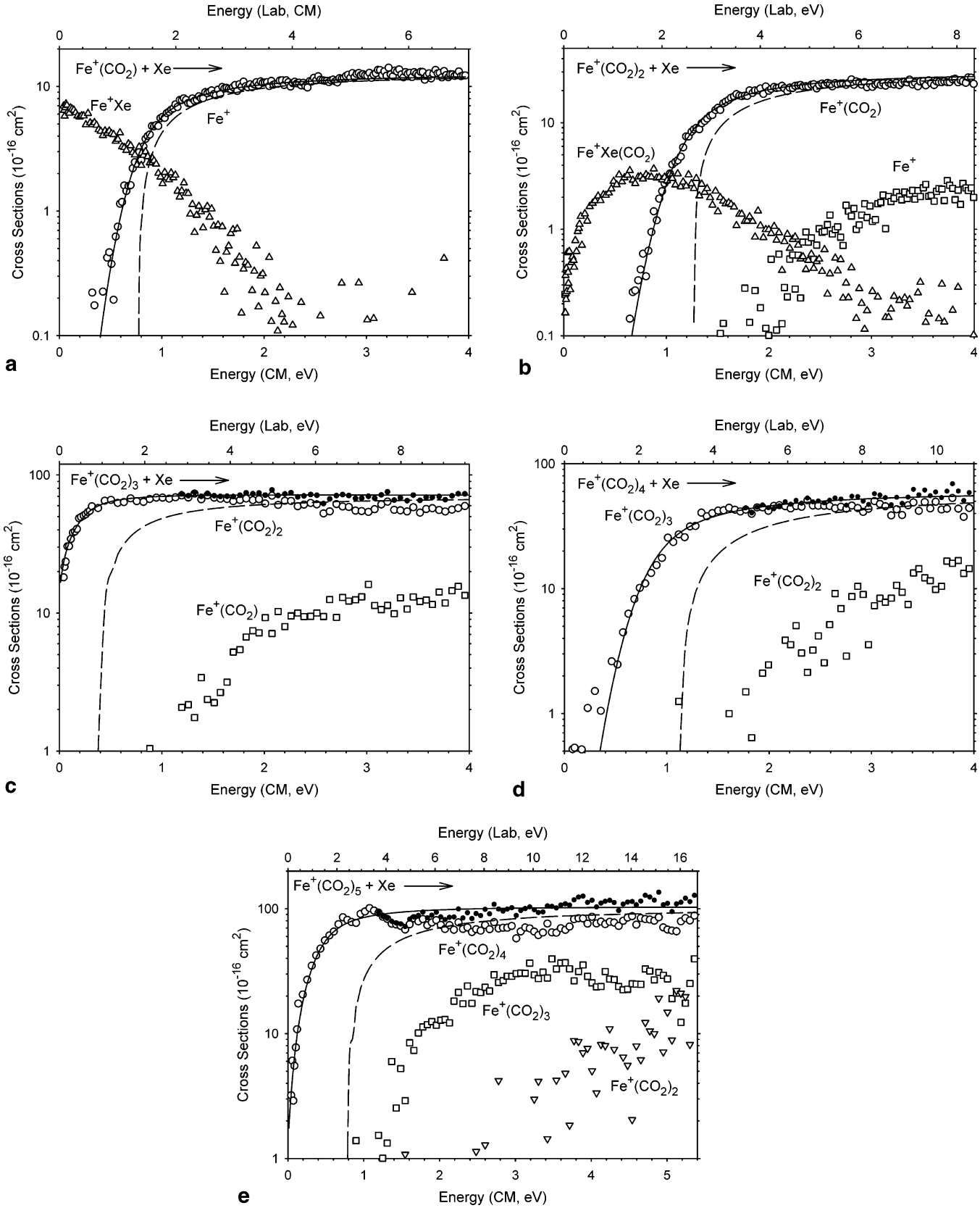

Figure 1. Cross sections for reactions of $Fe^+(CO_2)_n$, $n = 1-5$ (parts a−e, respectively), with xenon as a function of kinetic energy in the center-of-mass frame (lower *x* axis) and laboratory frame (upper *x* axis). The dashed lines show the model of eq 2 for reactants with no internal energy and in the absence of kinetic energy broadening. Solid lines are this model convoluted with the internal and kinetic energy distributions of the reactants. In parts c−e, the small dots show the total experimental cross section.

threshold near 0 eV and reaches a maximum magnitude of about 90 Å^2 at 1 eV. For this reaction, we also observe $Fe^+(CO_2)_3$ and $Fe^+(CO_2)_2$ product ions with apparent thresholds near 1 and 3 eV and maximum magnitudes of 30 and 10 Å^2, respectively. No other products are observed at any energy studied in these latter two systems.

3.2. Thermochemical and Threshold Analysis. The kinetic energy dependences of the experimental cross sections are

modeled using eq 2.[33]

$$\sigma(E) = (N\sigma_0/E)\sum g_i \int_{E_0-E_i}^{E} [1 - e^{-k(E^*)\tau}](E - \epsilon)^{N-1}\, d(\epsilon) \quad (2)$$

Here E is the relative translational energy of the reactants, N is an adjustable parameter that is related to the efficiency of the collisional energy transfer,[20] σ_0 is an energy-independent scaling factor, E_0 is the CID threshold at 0 K, τ is the experimental time for dissociation ($\sim 5 \times 10^{-4}$ s in the extended dual octopole configuration[20]), ϵ is the energy deposited in the complex by the collision, and E^* is the internal energy of the energized molecule (EM) after the collision, i.e., $E^* = \epsilon + E_i$. The sum is over the ro-vibrational states of the reactant ion, having energies E_i and populations g_i (where $\Sigma g_i = 1$). The vibrational frequencies of the complexes are determined at the BHandH/6-311+G* level of theory using Gaussian98W.[31] The Beyer−Swinehart algorithm[34−37] is used to calculate the distribution of internal states of the complexes at 300 K, the temperature of the gas in the flow tube. The term *k(E*)* is the unimolecular rate constant for dissociation, which is defined by Rice−Ramsperger−Kassel−Marcus (RRKM) theory, eq 3[37−40]

$$k(E^*) = d\, N^{\dagger}(E^* - E_0)/h\rho(E^*) \quad (3)$$

where d is the reaction degeneracy, $N^{\dagger}(E^* - E_0)$ is the sum of ro-vibrational states of the transition state (TS) at an energy $E^* - E_0$, and $\rho(E^*)$ is the density of states of the EM at the available energy, E^*.

To analyze the kinetic energy dependence of these cross sections and acquire accurate thermochemistry, several effects have to be considered. First, the internal energy of the reactants must be well-characterized. This is achieved by use of the flow tube ion source, which produces ion complexes with internal energy distributions that should be Maxwellian. As mentioned above, the cross sections at 0 eV collision energy are finite in the case of $Fe^+(CO_2)_3$ and nearly so for $Fe^+(CO_2)_5$. This implies that some ions have internal energies greater than the dissociation threshold. In the analysis of these data, such ions are assumed to have dissociated prior to reaching the collision cell. Second, the collision gas must provide efficient kinetic to internal energy transfer. Using Xe gas, which is heavy and polarizable while having no internal modes to carry away energy, satisfies this condition.[21,26] Third, rigorous single collision conditions are required to avoid problems associated with depositing excess (and unknown) energy in secondary collisions. To produce rigorous single-collision conditions, data obtained at different neutral reactant pressures ($\sim$ 0.05, 0.1, and 0.2 mTorr) are extrapolated to zero pressure by linear regression.[41] These are the cross sections shown in Figures 1.

Fourth, because the ions move through the apparatus in a finite time ($\sim 5 \times 10^{-4}$ s), it is important to consider the lifetime of dissociating ions, particularly for the larger complexes such as $Fe^+(CO_2)_3$, $Fe^+(CO_2)_4$, and $Fe^+(CO_2)_5$. As indicated in eq 2, the lifetime effect is taken into account using RRKM theory[37−40] in the phase space limit (PSL) using equations developed previously.[33] Briefly, the transition state (TS) for dissociation is modeled by loosely interacting products such that both fragments are free to rotate. This PSL is appropriate for ion−molecule complexes because the TS for the reverse, barrierless association process is accurately described as lying at the top of the centrifugal barrier. In this study, the two-dimensional (2-D) external rotations are treated adiabatically but with centrifugal effects included, consistent with the discussion of Waage and Rabinovitch.[42] The adiabatic 2-D rotational energy is treated using a statistical distribution with explicit summation over the possible values of the rotational quantum number, as described in detail elsewhere.[33]

TABLE 1: Parameters of Eq 2 Used to Model Data[a]

reactant ion	σ_0	N	E_0 (eV) no RRKM	E_0 (eV) with RRKM
$Fe^+(CO_2)$	16.1 (1.1)	0.9 (0.2)	0.77 (0.08)	0.77 (0.08)
$Fe^+(CO_2)_2$	43.7 (3.6)	0.8 (0.2)	1.27 (0.09)	1.26 (0.09)
$Fe^+(CO_2)_3$	77.0 (3.9)	1.0 (0.2)	0.40 (0.08)	0.38 (0.08)
$Fe^+(CO_2)_4$	71.4 (9.2)	1.2 (0.4)	1.05 (0.16)	0.93 (0.13)
$Fe^+(CO_2)_5$	116 (3)	0.9 (0.2)	0.85 (0.06)	0.71 (0.06)

[a] Uncertanties are listed in parentheses.

Because the rotational, vibrational, and translational energy distributions are explicitly included in our modeling, the threshold energies determined with eq 2 correspond to 0 K. By assuming that E_0 represents the energy difference between the reactants and products at 0 K,[21] threshold energies for CID reactions are equated with 0 K bond dissociation energies (BDEs). This correspondence is generally true for ion−molecule reactions because the presence of activation barriers in excess of the reaction endothermicity is unlikely,[43−46] especially for the simple heterolytic bond cleavages considered here.[47] The reported thresholds for all reactions are determined in the following way. First, eq 2 with an initial set of parameters is convoluted with the kinetic energy distribution of the ion beam and the thermal motion of the Xe gas in the reaction cell.[18] The parameters of eq 2 are optimized using a nonlinear least-squares analysis to give a best fit to the zero pressure extrapolated cross sections. Similar modeling that includes the PSL analysis to estimate lifetime effects[33] is also performed and shown for all five complexes in Figure 1. It can be seen that these models reproduce the experiments accurately over extended energy and magnitude ranges. The optimized values for E_0 obtained with lifetime effects represent the bond energies of interest at 0 K. An estimate of the absolute uncertainty in the threshold energy is obtained by variations in the parameter N in eq 2, variations in the time available for reaction by factors of 2 and $^1/_2$, variations in the vibrational frequencies of the reactant and TS by $\pm$10%, and the error in the absolute energy scale ($\pm$0.05 eV lab). Threshold energies, both with and without lifetime effects, along with the optimum fitting parameters, σ_0 and N, for all reactions studied here are listed in Table 1.

3.3. Theoretical Structures. The theoretical structures of the $Fe^+(CO_2)_n$ complexes were calculated at the BHandH/6-311+G* level. Fe^+ ion and CO_2 bind electrostatically where the leading term results from interaction of the ion with the quadrupole moment of CO_2. Because CO_2 has a negative quadrupole moment, CO_2 prefers end-on coordination.[9,10] This coordination geometry is found for all ligands in all complexes but $Fe^+(CO_2)_5$, see below. The possible spin states (sextet, quartet, and doublet) for each complex were carefully investigated and Table 1S lists the energies, zero point energies, and rotational and vibrational constants of the $Fe^+(CO_2)_n$ complexes for which converged structures could be found at this level of theory. Table 2S lists the geometrical parameters for each of these $Fe^+(CO_2)_n$ complexes. In several cases, these complexes have geometries slightly distorted from more symmetric orientations. Repeated attempts to locate these higher symmetry minima were made and included the use of finer integration grids, but were unsuccessful.

Sextet States. Stable sextet state geometries were found for the $Fe^+(CO_2)_n$ ($n = 1-3$) complexes, Figure 2. These evolve by attaching ligands to the $Fe^+(^6D, 4s^13d^6)$ ground state. For

TABLE 2: 0 K Bond Dissociation Energies (eV) for $(L)_{n-1}Fe^+-L$ Complexes Where L = CO_2, CO, and N_2

	CO_2				CO		N_2
		theory[b]					
ligand	exptl[a]	BH&H	B3LYP	CCSD(T)	exptl[c]	theory[d]	exptl[e]
Fe^+-L	0.77 ± 0.08	0.89	0.69	0.64	1.34 ± 0.04	1.35	0.56 ± 0.06
	0.62 ± 0.04[f]	0.58−0.80[h]	0.90[h]	0.76[i]			
	0.56 ± 0.08[g]						
$(L)Fe^+-L$	1.26 ± 0.09	1.20[j]	0.95[j]	0.83[j]	1.53 ± 0.05	1.60	0.86 ± 0.09
$(L)_2Fe^+-L$	0.38 ± 0.08	0.57	0.37		0.71 ± 0.06	0.78	0.47 ± 0.06
$(L)_3Fe^+-L$	0.93 ± 0.13	0.62	0.40		1.01 ± 0.06	0.98	0.56 ± 0.04
$(L)_4Fe^+-L$	0.71 ± 0.06	0.20			1.00 ± 0.04	0.83	0.64 ± 0.04

[a] This work, except as noted. [b] This work, except as noted. [c] References 12 and 14. [d] B3LYP calculations.[51] For $Fe^+(CO)$, dissociation energy along the quartet surfaced was corrected for experimental splitting to $Fe^+(^6D)$ ground state. [e] Reference 14. [f] Reference 8. [g] Reference 7, revised to 0.63 ± 0.08 eV in ref 8. [h] Reference 10. Values in BH&H column are MP2 values. [i] CCSD(T)/ANO level of theory, Reference 9. [j] Values for adiabatic dissociation, see text. Spin-allowed dissociation values are 1.27, 0.99, and 1.06 eV for BH&H, B3LYP, and CCSD(T) levels, respectively.

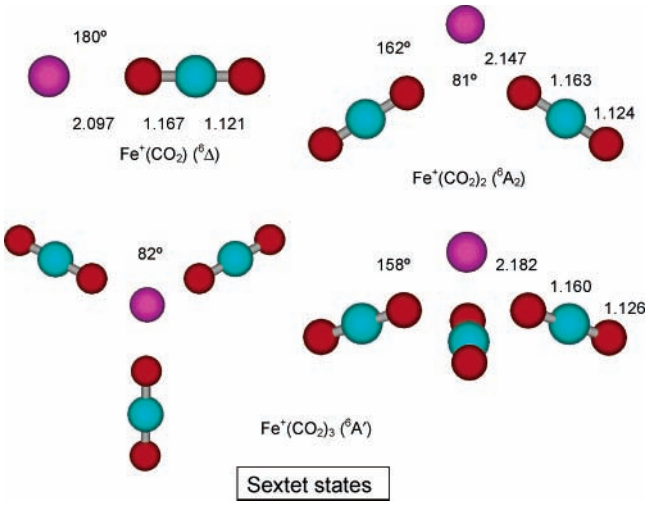

Figure 2. Structures of the sextet states for $Fe^+(CO_2)_n$, $n = 1-3$, optimized at the BHandH/6-311+G* level of theory.

the monoligated species, two states are found, $^6\Delta$ and $^6\Pi$, both with linear geometries. These correspond to having the doubly occupied 3d orbital on iron be the $3d\delta$ or $3d\pi$, respectively, and have relative energies after ZPE corrections of 0.000 and 0.083 eV, respectively. This indicates that the relative order of the 3d orbitals on Fe^+ is $3d\delta < 3d\pi < 3d\sigma$, which is determined by the overlap with the occupied orbitals of CO_2, as previously pointed out by Sodupe et al.[9] The pertinent π orbital on the CO_2 ligand is the π_g nonbonding orbital, such that this interaction does not change the O−CO bond length appreciably, Table 2S. Thus, the FeO−CO bond lengths are longer than O−CO bond length by about 0.02 Å, which exceed the FeOC−O bond lengths by about 0.02 Å, Table 2S. This trend is continued for all complexes of all spin states and is similar to the observations made for $M^+(CO_2)$ complexes of all first row transition metal cations.[9,10] Overall, there is no significant π-back-donation from the metal ion to the CO_2 ligand.[9]

When a second CO_2 ligand is added to the complex, it adopts a bent geometry. Four sextet states were identified, $^6A_2$, $^6A_1$, $^6B_1$, and $^6B_2$, with similar geometries and relative energies of 0.00, 0.030, 0.048, and 0.356 eV, respectively. With the C_2 symmetry axis identified as the *z* axis, these states correspond to the doubly occupied 3d orbital residing in the $3d_{xy}$, $3d_{x^2-y^2}$, $3d_{yz}$ (out of plane), and $3d_{xz}$ (in plane). The latter orbital points directly at the ligands, explaining why the $^6B_2$ state is so much higher in energy. Qualitatively, the geometry of the $Fe^+(CO_2)_2$ complex is directly analogous to that previously characterized for $Mg^+(CO_2)_2$.[48] Mg^+ also has a single valence electron in an s orbital, and therefore the explanation for these geometries is parallel.[49] Specifically, the high-spin state of $Fe^+(^6D)$ requires that the 4s orbital remain occupied. As this orbital is the largest valence orbital, it interacts with the incoming ligands strongly. To avoid repulsion with the incoming ligands, 4s−4p polarization is induced such that the electron occupies a sp hybrid orbital located away from the incoming ligands. In simplistic terms analogous to the valence shell electron pair repulsion model (VSEPR),[50] this electron occupies a ligand site such that the $Fe^+(CO_2)_2$ complex can be thought of as nearly having a trigonal planar geometry with the hybridized 4s electron occupying one of these sites. Note that the CO_2 ligands are not aligned directly with the Fe^+ ($\angle$FeOC = 162−168°, Table 2S) because the electron density is being donated to the empty sp hybrid orbital formed.

This same analysis holds for the $Fe^+(CO_2)_3$ complex, which can be thought of as a distorted tetrahedral arrangement of the three ligands and one valence electron. This again matches the geometry found for the analogous magnesium ion complex, $Mg^+(CO_2)_3$.[48] Again the ligands are directed at the empty sp hybrid orbital ($\angle$FeOC = 158°). Only one state was characterized for this species, a $^6A'$ state. The geometry located is slightly distorted from having a C_3 rotational axis, although a more symmetric structure is unlikely to be much lower in energy.

A sextet state for the $Fe^+(CO_2)_4$ complex was briefly explored but was clearly much higher in energy than lower spin states and hence optimizations of this complex and of $Fe^+(CO_2)_5$ were not pursued further.

Quartet States. For ligation of $Fe^+(^4F, 3d^7)$, the absence of the 4s electron makes the geometries more symmetric. Thus, ligation with one, two, three, and four CO_2 ligands yields geometries that have linear, linear, distorted trigonal planar, and distorted tetrahedral geometries, Figure 3. For $Fe^+(CO_2)$, the $^4\Delta$ state has a shorter Fe−O bond distance than the $^6\Delta$ state, Table 2S, consistent with reduced repulsion between the 4s electron and the ligand. This state has a valence electron configuration on the iron atom of $\sigma^2\pi^2\delta^3$ where the σ orbital is a $4s + 3d\sigma$ hybridized orbital perpendicular to the bonding axis. Again the $3d\pi$ orbitals prefer to be half-filled as a result of the interaction with the occupied π_g orbitals on the CO_2 ligand.

For the bisligated system, three states all having linear geometries were located. The ground state is $^4\Delta$, with a $^4\Phi$ lying 0.123 eV higher in energy and a $^4\Sigma^-$ lying 1.098 eV above the ground state. All three states have similar bond lengths although the $^4\Delta$ ground state has the shortest Fe−O bond lengths by a small margin, Table 2S. These states correspond to valence electron configurations on the iron atom of $\sigma^2\pi^2\delta^3$, $\sigma^1\pi^3\delta^3$, and $\sigma^1\pi^2\delta$,[4] respectively, where again the σ orbital is a $4s + 3d\sigma$ hybrid. Note that the Fe−O bond lengths in the $^4\Delta$ state of $Fe^+(CO_2)_2$ are shorter than those for the $^4\Delta$ state of $Fe^+(CO_2)$,

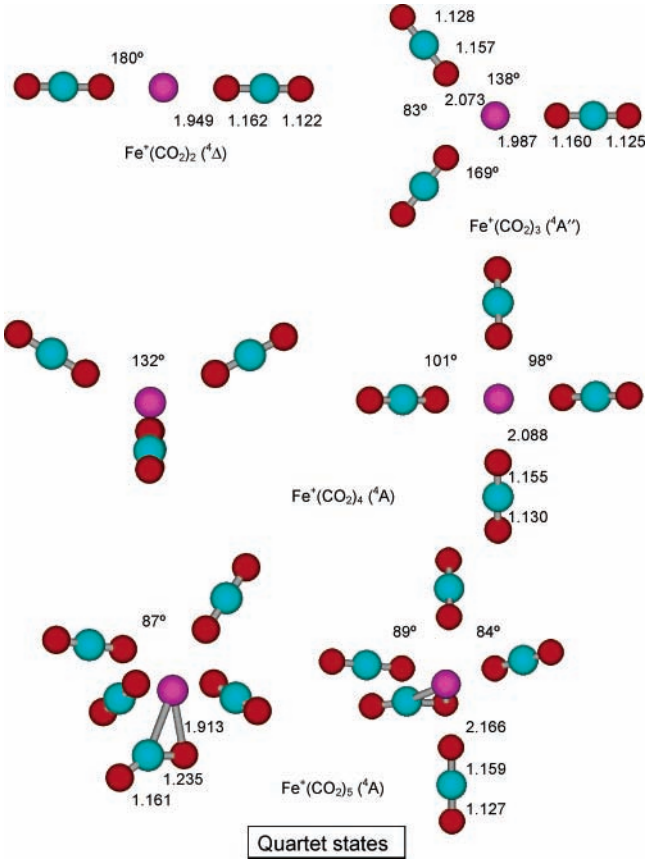

Figure 3. Structures of the quartet states for $Fe^+(CO_2)_n$, $n = 2-5$, optimized at the BHandH/6-311+G* level of theory.

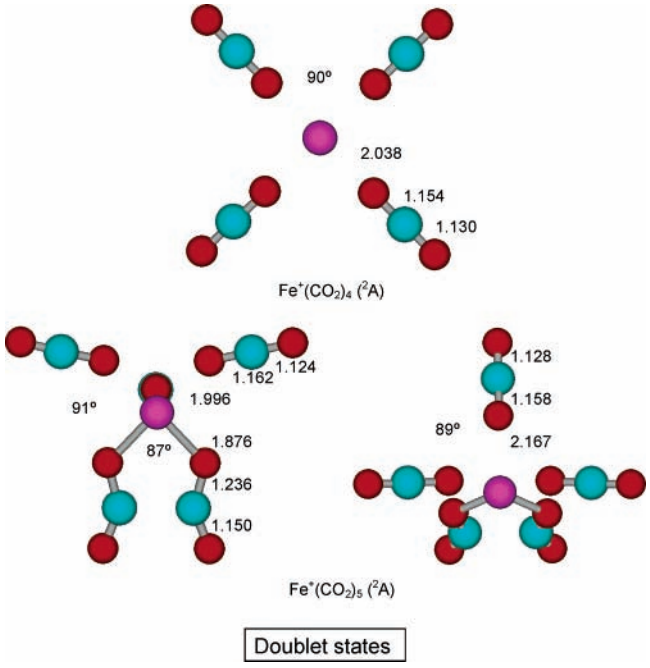

Figure 4. Structures of the doublet states for $Fe^+(CO_2)_n$, $n = 4$ and 5, optimized at the BHandH/6-311+G* level of theory.

indicating that the 4s + 3dσ hybridization is more effective with two ligands inducing this polarization. The balance between keeping the 3dσ and 3dπ orbitals half empty leads to the near degeneracy of the $^4\Delta$ and $^4\Phi$ states. Given this, it seems odd that the $^4\Sigma^-$ state, which has both the 3dσ and 3dπ orbitals half empty, is not lower in energy, but this is because the $^4\Delta$ and $^4\Phi$ states both evolve from a pure ^{4}F state of Fe^+, whereas the $^4\Sigma^-$ orbital configuration correlates with Fe^+ composed of 20% ^{4}F and 80% ^{4}P. The ^{4}P state lies 1.388 eV higher in energy (80% of 1.388 eV = 1.110 eV, comparable to the calculated excitation energy).[27]

Only one quartet state was found for the $Fe^+(CO_2)_3$ system. The geometry is planar with a ^{4}A″ ground state (the B3LYP approach finds a more symmetric C_{2v} geometry and a $^4A_2$ state). This planar geometry is in sharp contrast to the analogous sextet state, however, the ligands are not symmetrically arrayed around the central iron atom. This is a result of the 4s−3dσ hybridization which places electron density perpendicular to the axis of the ligands in the $Fe^+(CO_2)_2$ complex. This leaves the other 4s−3dσ hybrid, which lies along the axis, empty, and is thus able to accept electron density from the ligands. Apparently, addition of a third ligand is not sufficient to disrupt the energetic advantage of this hybridization, such that two CO_2 ligands interact with the Fe^+ on the side opposite the third ligand. Presumably the geometry is limited by steric interactions between these two ligands such that the OFeO angle is 83°, Table 2S, similar to the angles in the sextet states. Note too that these two ligands have longer FeO bond distances than the unique ligand (2.073 vs 1.987 Å). The energetic advantage of retaining the 4s−3dσ hybridization is also maintained in the $Fe^+(CO_2)_4$ complex. Here, two pairs of ligands have OFeO angles distorted from the tetrahedral ideal of 109.5°, such that they lie closer together at 98°. At the BHandH level, the $Fe^+(CO_2)_4$ complex has no symmetry, whereas the B3LYP level finds a plane of symmetry and a ^{4}A″ ground state.

The geometry of the $Fe^+(CO_2)_5$ complex is unique among those calculated here. Extensive searches for other stable geometries were made starting with both square planar and trigonal bipyramidal structures, but the only stable complex found was that shown in Figure 3. Ultimately the ability to explore configurational space is limited by the weak bonding in this complex and the ease with which the CO_2 ligands can rotate. This structure can be viewed as starting from a trigonal bipyramid but one of the equatorial ligands is now π-bonding to the Fe^+. The geometry found is very close to having C_s symmetry with the π-bonding CO_2 and two other ligands lying in the plane of symmetry.

Doublet States. Doublet spin states of the $Fe^+(CO_2)_4$ and $Fe^+(CO_2)_5$ complexes were both found and are shown in Figure 4. The tetraligated complex is planar with C_{4h} symmetry (close to D_{4h}), with the only distortions being the FeOC bond angles of 179.1° rather than 180.0°. Although the wave function for the symmetric D_{4h} complex would not converge at the level chosen, other levels of theory might find this as the true minimum structure.

As for the quartet state of $Fe^+(CO_2)_5$, extensive geometry optimizations starting from symmetric starting points were tried but the only stable complex found is that shown in Figure 2. Here two of the CO_2 ligands begin to interact through the carbon atoms, giving a C−C distance of 1.963 Å, and the shortest FeO bond distances, 1.876−1.878 Å. The three loosely bound CO_2 ligands have a T-shape array with the central ligand having the longest FeO bond distance, 2.167 Å. The molecule nearly has a plane of symmetry with only very small distortions.

It was anticipated that the largest complexes would exhibit the most stable doublet spin states. Hence, doublet states for smaller complexes, $Fe^+(CO_2)_n$ ($n = 1 - 3$), were not explored because it was clear they would be high lying excited states.

3.4. Experimental and Theoretical Bond Dissociation Energies. The 0 K bond dissociation energies (BDEs) for $Fe^+(CO_2)_n$ measured experimentally are 0.77 ± 0.08, 1.26 ±

0.09, 0.38 ± 0.08, 0.93 ± 0.13, and 0.71 ± 0.06 eV for n = 1−5, respectively (Table 1). Small lifetime effects (≤0.02 eV) are observed for n = 1−3, which seems reasonable because the complexes have few degrees of freedom. The lifetime effects are larger (~0.13 eV) for n = 4 and 5. Previously, we measured the threshold for CID of $Fe^+(CO_2)$ with Xe as 0.66 ± 0.05 eV.[6] The present result is slightly higher, although within combined experimental errors. The difference comes from the smaller value of the fitting parameter n (0.9 vs 1.2), which allows us to fit the Fe^+ product ion cross section over a wider energy range (up to 3 eV, whereas the previous model cross section fit only up to 1.5 eV). The final bond energy determined in our previous work, 0.62 ± 0.04 eV, was the result of a series of interdependent CID and ligand exchange processes.[8] This remains our best value, although the present experimental results suggest a slightly higher value.Strong BDEs are observed for the second and fourth CO_2 ligands with the second BDE being the strongest, and the weakest BDE is for the third CO_2. These experimental BDEs for $Fe^+(CO_2)_{n-1}-CO_2$ are summarized in Table 2 along with the theoretical BDEs obtained at BHandH, B3LYP, and CCSD(T) levels of theory and literature values. As mentioned above, the BHandH level of theory predicts the ground state of Fe^+ as sextet. The ground state for $Fe^+(CO_2)$ is also sextet at the BHandH level of theory in agreement with the CCSD(T)/ANO result of Sodupe et al.[9] and our CCSD(T) calculation. The energy difference between the sextet ground state and quartet excited state at the CCSD(T)/ANO level of theory is 0.056 eV, comparable to the 0.072 eV excitation energy calculated here at the BHandH level of theory, but somewhat smaller than our CCSD(T) value of 0.239 eV. In contrast, literature B3LYP calculations[9] predict a quartet ground state by 0.16 eV, and our B3LYP calculations yield a quartet ground state with a sextet excitation energy of 0.415 eV. Sodupe et al. note that if the relative energies are corrected for the incorrect ordering of the atomic states of Fe^+, a sextet ground state for $Fe^+(CO_2)$ is again predicted at the B3LYP level. In any event, the calculated bond energies for $Fe^+(CO_2)$ range from about 0.6 to 0.9 eV, which is also the range of the experimental values. For present purposes, we note that the present BHandH value, 0.89 eV, appears somewhat high compared to experiment and most other levels of theory.

At the BHandH level of theory, all $Fe^+(CO_2)_n$ complexes except n = 1 have ground states with quartet spin. This means that the lowest energy channel for loss of a single ligand from all complexes except n = 2 are spin allowed. For dissociation of $Fe^+(CO_2)_2$, the complex can dissociate adiabatically in a spin-forbidden pathway or along the spin-allowed pathway forming an excited quartet state of $Fe^+(CO_2)$. Ultimately, this does not make a large difference in the predicted bond energies as the excitation energies of the $Fe^+(CO_2)$ ($^4\Delta$) state are only 0.07, 0.24, and 0.04 eV at the BHandH, CCSD(T), and B3LYP levels, respectively (where the latter value has been adjusted to provide the correct ^{6}D-^{4}F splitting of Fe^+). Thus, the experimental BDE of 1.26 ± 0.09 eV agrees well with both the adiabatic (1.20 eV) and spin-allowed (1.27 eV) bond energies predicted at the BHandH level. The B3LYP values, 0.95 and 0.99 eV, respectively, are both too low compared to experiment, as are the CCSD(T) predictions of 0.83 (adiabatic) and 1.06 eV (spin-allowed). Overall, the comparison between theory and experiment does not definitely address whether the bond energy measured experimentally is the adiabatic or spin-allowed process. Comparison with other complexes of Fe^+ suggests that it may be the spin-allowed process, as described further below. If so, then the 1.26 ± 0.09 eV value should be lowered by the excitation energy of the $Fe^+(CO_2)$ quartet to yield the true adiabatic value.

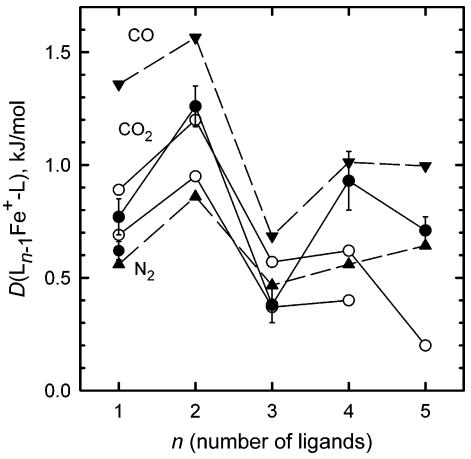

Figure 5. Sequential bond energies (in eV) for CO_2 (circles), CO (inverted triangles), and N_2 (triangles) bound to iron ion. Experimental values are shown by solid symbols, whereas open symbols indicate theoretical values (upper values: BHandH/6-311+G*; lower values: B3LYP/6-311+G*). Data are taken from Table 2.

Comparison of the BHandH and B3LYP BDEs for n = 1−4 shows that they exhibit the same variations as the number of ligands is varied, Figure 5, although the B3LYP values are weaker by an average of 0.22 ± 0.02 eV. The strongest BDE at both levels of theory is observed for n = 2 and the weakest BDE is observed for n = 3, consistent with our experimental results. The relative weakness of the BDE for $Fe^+(CO_2)_3$ is confirmed unequivocally by the qualitative behavior of the cross sections, Figure 1. The theoretical BHandH BDEs increase from n = 3 to n = 4, and then drop for n = 5, in qualitative agreement with the experimental BDEs. Although B3LYP theory reproduces the $(CO_2)_2Fe^+-CO_2$ BDE, BHandH theory overestimates the experimental value for n = 3, and both DFT approaches underestimate the BDEs for n = 4 and 5. Note that the sums of the third and fourth BDEs agree reasonably well, 1.31 ± 0.15 (experiment) vs 1.19 eV (BHandH theory), although B3LYP predicts a lower sum of 0.77 eV. The agreement may suggest that the $Fe^+(CO_2)_3$ complex is not adequately described by theory but $Fe^+(CO_2)_4$ is. Alternatively, the agreement of the B3LYP BDE for $Fe^+(CO_2)_3$, 0.37 eV, and the experimental value of 0.38 ± 0.08 eV suggests that the BHandH values are somewhat high and that theory incorrectly describes $Fe^+(CO_2)_4$. The large discrepancy between the experimental and theoretical BDEs for $Fe^+(CO_2)_5$ probably indicates that the true minimum was not found theoretically, which is not surprising given the difficulty in adequately exploring this floppy molecule. Overall, our experimental values are in reasonable agreement with the BHandH density functional theory results except for n = 5 and with B3LYP density functional theoretical results for n = 1−3.

4. Discussion

4.1. Trends in Bonding. In all $Fe^+(CO_2)_n$ complexes, the M^+O-CO bond length is slightly longer than the O−CO bond length in free CO_2, which is slightly longer than the M^+OC-O bond length. As noted above, this is a consequence of the interaction of the occupied Fe^+ ($3d\pi$) and CO_2 (π_g) orbitals. A long Fe^+-OCO bond length (2.14, 2.10, and 2.18 Å) for the $^6\Delta$ state is observed at B3LYP,[9] BHandH, and B3LYP levels of theory, respectively. The Fe^+-OCO bond length (2.03, 2.00, and 2.04 Å) for the $^4\Delta$ state is shorter than that in the sextet ground state. This shorter bond length is a consequence of

4s−3dσ hybridization. The 4s + 3dσ hybrid localized along the bonding axis is left empty to act as an acceptor orbital for electron density from the ligand. The electrons originally in the dσ orbital occupy the 4s−3dσ orbital localized perpendicular to the bonding axis. Thus, hybridization reduces the electron density of the metal along the bonding axis, thereby reducing metal−ligand repulsion and increasing the effective nuclear charge seen by the ligand. In contrast, the high-spin sextet state requires that both 4s−3dσ hybrids must be occupied, such that the orbital localized along the bonding axis is at least singly occupied. Thus, 4s−3dσ hybridization is not useful in increasing the binding for the sextet state. Despite the stronger interaction between $Fe^+(^4F)$ and CO_2 (as indicated by the shorter Fe−O bond length, Table 2S), the overall energy of the quartet complex is still higher than the sextet because it is formed from an excited-state asymptote.

The second CO_2 binds much more strongly than the first. This is consistent with the infrared photodissociation study by Gregoire and Duncan, who reported that $Fe^+(CO_2)_2$ appears to be particularly stable.[11] This can again be explained by 4s−3dσ hybridization. Because of the symmetry of the 4s−3dσ hybrid orbitals, a second ligand, located 180° away from the first, can donate electrons to the same empty, on-axis 4s + 3dσ hybrid orbital. Thus, the second ligand also feels less repulsion and a higher nuclear charge, whereas the energetic cost of hybridization and promotion to the quartet state is shared by two ligands. Hence, the BDE of the second ligand is stronger than that of the first. This is also demonstrated by noting that the $^4\Delta$ ground state of $Fe^+(CO_2)_2$ at the BHandH and B3LYP levels of theory shows a linear structure with shorter Fe^+−OCO bond lengths (1.95 and 2.01 Å) than the $^4\Delta$ state of $Fe^+(CO_2)$ (2.00 and 2.04 Å). As in $Fe^+(CO_2)$, 4s−3dσ hybridization is effective for the quartet state but not the sextet state because the 4s + 3dσ orbital localized along the bonding axis is occupied for the sextet state. This forces the sextet states of this complex to adopt a bent geometry (OFeO bond angles of 79−86°) leading to more ligand−ligand repulsive interactions, which destabilize this complex relative to the quartet state (excitation energies of 0.53−0.89 eV at the BHandH level).

For $Fe^+(CO_2)_3$, our calculations at the BHandH level of theory indicate the quartet $Fe^+(CO_2)_3$ complex is lower in energy by 0.53 eV compared to the sextet minimum. The quartet complex has two weakly bound ligands located on the other side of a tightly binding CO_2, as indicated by Fe−O bond lengths of 2.07 Å and 1.99 Å, respectively. These two more loosely attached CO_2 ligands form an acute OFeO angle of 83°, whereas the other two OFeO angles are 138°, Figure 3. Although the $Fe^+(CO_2)_3$ complex retains 4s−3dσ hybridization, the ligand−ligand repulsive interactions between the two loosely bound CO_2 ligands limits the OFeO bond angles and prevents these two loosely binding CO_2 from approaching the Fe^+ ion more closely. Therefore, the third CO_2 results in a weaker BDE.

A relatively strong experimental BDE is observed for the fourth CO_2. The structure of the quartet ground state of $Fe^+(CO_2)_4$ at the BHandH level is a distorted tetrahedron. All Fe^+−OCO bond lengths are nearly identical (2.09 Å) but the OFeO bond angles are 98° (2), 101° (2), and 132° (2), Table 2S. As pointed out for the $Fe^+(CO)_4$ complex,[51] the BDE for the fourth ligand can be stronger than the third because four ligands now share the energetic loss of 4s−3dσ hybridization, while the fourth ligand changes the metal−ligand interactions very little and ligand−ligand repulsions increase only slightly. The theoretical BDEs for the fourth CO_2 ligand underestimate the experimental BDE by 0.3−0.5 eV. More sophisticated theory (perhaps a complete active space multiconfiguration SCF, CASSCF) is required to solve this discrepancy. The doublet state of $Fe^+(CO_2)_4$ is calculated to lie 1.25 eV above the quartet ground state, too high to be important in the experiments.

For the $Fe^+(CO_2)_5$ complex, we find a minimum on the quartet state surface at the BHandH level of theory which shows one of the CO_2 ligands attached to Fe^+ ion in a nearly "T" shaped fashion. At the BHandH level, the doublet state of $Fe^+(CO_2)_5$ is 1.68 eV higher than the quartet minimum, again making it unimportant experimentally. Our theoretical BDE for dissociation of quartet state $Fe^+(CO_2)_5$ to quartet $Fe^+(CO_2)_4$ is only 0.20 eV, which severely underestimates the experimental BDE. Experimentally, the qualitative behavior of the cross sections, Figure 1, shows that this BDE must exceed that for $Fe^+(CO_2)_3$, in contrast to the theoretical predictions. As in the $Fe^+(CO_2)_4$ case, more sophisticated theory is required to solve this discrepancy.

4.2. Comparison to Other Iron Ion Complexes. Tjelta and Armentrout[14] compared the sequential BDEs of Fe^+ ion with π-accepting ligands (N_2,[14] CO,[12] and H_2[16]) and π-donating ligands (CH_2O[14] and H_2O[13]). In all cases, the bond to the second ligand is the strongest and that to the third ligand is relatively weak. However, for the fourth ligand, π-accepting ligand systems exhibit relatively strong BDEs, whereas the BDEs observed for π-donating ligand systems are weaker than the third. Furthermore, π-donating ligands do not easily form $Fe^+(L)_5$ complexes whereas these are observed for the π-accepting ligands. Clearly, the pattern observed here for CO_2 ligands is consistent with that of the π-accepting ligands, even though the electronic structure calculations do not indicate strong π interactions between Fe^+ and CO_2.[9] In general, we find that the BDEs of CO_2 are weaker than those for CO and stronger than those for N_2, such that the CO_2 BDEs average 71 ± 16% of the CO BDEs compared to N_2, which averages BDEs only 57 ± 11% of the CO BDEs.

Qualitatively, the difference between the π-donating and π-accepting ligands can be rationalized by considering the $Fe^+(L)_4$ species. π-Accepting ligands prefer a square planar geometry that makes the doubly occupied d orbitals of *xy*, *xz*, and *yz* symmetry available for back-donation. π-Donating ligands prefer a tetrahedral geometry in which these orbitals are singly occupied, such that they can accept electron density. These considerations indicate that the tetrahedral species will have a quartet spin state, whereas a square planar species will ordinarily prefer to be in a doublet spin state. Indeed, calculations of Ricca and Bauschlicher on $Fe^+(CO)_4$ complexes find these symmetric species and verify that the square planar complex has a doublet ground state and the tetrahedral geometry has quartet spin.[51] These calculations are unable to distinguish which of these states is the ground state of this complex. Likewise, our calculations find that the doublet state of $Fe^+(CO_2)_4$ has a square planar geometry, and the quartet ground state has a distorted tetrahedral geometry with OFeO bond angles of 98° (2), 101° (2), and 132° (2) with essentially uniform Fe−O bond lengths of 2.09 Å (4). A somewhat similar distorted geometry has been calculated for the quartet state of $Fe^+(H_2O)_4$ by Ricca and Bauschlicher,[52] where the OFeO bond angles are 79° (2), 110° (2), 142°, and 154° with nonuniform FeO bond lengths of 2.113 (2) and 2.235 (2) Å. Apparently, the fact that CO_2 is neither a strong π-donor nor π-acceptor leads to this intermediate distortion.

This intermediate character is also found for the geometries of the quartet states of $Fe^+(CO_2)_3$ vs $Fe^+(CO)_3$[51] and $Fe^+(H_2O)_3$.[52] Whereas the $Fe^+(CO)_3$ complex has trigonal planar symmetry,

TABLE 3: Theoretical and Experimental Shift of CO_2 Asymmetric Stretch Frequencies and Relative IR Intensities

		shift (cm^{-1})[a]	
species	state	theoretical[b]	experimental[c]
$Fe^+(CO_2)$	$^6\Delta$	31 (1.0)	34 [3][d]
	$^6\Pi$	27 (1.0)	
	$^4\Delta$	40 (1.0)	42 [2][d]
$Fe^+(CO_2)_2$	$^6A_2$	−2 (1.0), 37 (0.3)	∼0 (0.6)
	$^6A_1$	11 (1.0), 34 (0.4)	
	$^6B_1$	27 (1.0), 34 (0.5)	
	$^6B_2$	3 (1.0), 24 (0.5)	
	$^4\Delta$	38 (1.0), 52 (F)	40 (1.0)
	$^4\Sigma^-$	37 (1.0), 52 (F)	
	$^4\Phi$	32 (1.0), 49 (F)	
$Fe^+(CO_2)_3$	$^6A'$	−8 (1.0), 6 (0.7), 40 (0.1)	
	$^4A''$	15 (0.8), 27 (1.0), 48 (0.0)	∼20 (0.3), 27 (1.0), ∼50 (0.3)
$Fe^+(CO_2)_4$	$^4A''$	13 (0.6), 16 (1.0), 16 (1.0), 49 (0.0)	18 (1.0), ∼30 (0.2)
	^2A	12 (0.0), 23 (1.0), 24 (1.0), 59 (0.0)	
$Fe^+(CO_2)_5$	^4A	12 (0.4), 16 (1.0), 17 (0.8), 49 (0.1)	17 (1.0), ∼36 (0.2)
	^2A	16 (0.6), 21 (1.0), 49 (0.1)	

[a] Shift from the free CO_2 asymmetric stretch vibrational frequency at 2349 cm^{-1}. [b] Values calculated at the BHandH/6-311+G* level of theory after scaling by 0.916 to bring the predicted frequency for free CO_2 into accord with experiment. Numbers in parentheses indicate the relative IR intensities calculated. F indicates a forbidden transition. [c] Values from Gregoire and Duncan.[11] Numbers in parentheses indicate the relative IR intensities measured. [d] Values in brackets indicate the number of Ar atoms attached to $Fe^+(CO_2)$.

indicating the complete loss of 4s−3dσ hybridization, the $Fe^+(H_2O)_3$ complex has OFeO bond angles of 80 and 140° (2) with a short FeO bond distance and two long ones that differ by 0.098 Å. This is similar to bond angles of 83 and 138° (2) and FeO bond distance differentials of 0.086 Å for $Fe^+(CO_2)_3$.

It can be noted that the increase in bond energies between $n = 1$ and 2 is larger for the CO_2 complexes than for either CO or N_2 complexes, Table 2 and Figure 5. This is plausibly because the measured bond energy for $Fe^+(CO_2)_2$ corresponds to the spin-allowed process forming an excited quartet state of $Fe^+(CO_2)$. The adiabatic bond energy would be lower by this excitation energy, calculated to be 0.07, 0.24, and 0.04 eV at the BHandH, CCSD(T), and B3LYP (corrected for the incorrect state splittings of Fe^+), respectively.

4.3. Infrared Spectroscopy of $Fe^+(CO_2)_x$ Complexes. At the time Gregoire and Duncan[11] published their IR dissociation study, no theory had been performed on complexes larger than $Fe^+(CO_2)_2$. The present calculations now provide vibrational frequencies and IR intensities that can be compared to the spectra of Gregoire and Duncan. In all cases, the antisymmetric stretch frequency of CO_2 is the focal point of the spectroscopic studies. Both theoretical (BHandH) and experimental results for the shift in this frequency from that for free CO_2 are given in Table 3 along with the relative intensities of each band. B3LYP results are similar to the BHandH results in all cases.

For $Fe^+(CO_2)$, no direct IR photodissociation was observed and only spectra of $Fe^+(CO_2)Ar_2$ and $Fe^+(CO_2)Ar_3$ were obtained. These each exhibited a single strong absorption blue-shifted from the free CO_2 line by 42 and 34 cm^{-1}, respectively. Gregoire and Duncan extrapolated these values to a hypothesized shift of 58 cm^{-1} for $Fe^+(CO_2)$. Our calculations indicate that the $^6\Delta$ state of $Fe^+(CO_2)$ has an asymmetric stretch blue-shifted by 31 cm^{-1} (identical to the shift predicted by calculations of Brinckman and Schaefer[53]), whereas the $^4\Delta$ state has a shift of 40 cm^{-1}. Gregoire and Duncan discounted the theoretical predictions, which is still possible, but the good agreement of our calculated results for larger complexes (see below) leads us to consider another explanation. The agreement between the observed spectra and the predicted spectra is excellent if the $Fe^+(CO_2)Ar_2$ and $Fe^+(CO_2)Ar_3$ complexes are presumed to correspond to the $^4\Delta$ and $^6\Delta$ states, respectively. It is possible that addition of two Ar ligands to the $Fe^+(CO_2)$ complex could preferentially stabilize the quartet state relative to the sextet state, however, it seems unlikely that addition of a third would switch the ground state back to the sextet state. Therefore, we postulate that one of the spectra is actually anomalous in some fashion, although it is unclear which spectrum is incorrect.

The spectrum for $Fe^+(CO_2)_2$ is notable because it differs greatly from the spectra of the larger complexes. A strong sharp band is found at 2389 cm^{-1}, a blue-shift of 40 cm^{-1} from the free CO_2 band. A broad band centered near the free CO_2 stretch frequency of 2349 cm^{-1} is also observed and postulated to be a consequence of a minor isomer with the CO_2 bound side-on or not attached directly to the metal. The present calculations suggest an interesting alternative explanation. Specifically, our calculations predict that the $^4\Delta$ ground state of $Fe^+(CO_2)_2$ should have a single intense band blue-shifted by 37 cm^{-1} from free CO_2, in excellent agreement with the main feature in the observed spectrum, with a second band shifted by 52 cm^{-1} being IR inactive. However, the sextet states of $Fe^+(CO_2)_2$ are predicted to exhibit a strong band near the free CO_2 value, shifts of −2 ($^6A_2$), 11 ($^6A_1$), and 27 ($^6B_1$) cm^{-1}, with a weaker band shifted by 34−37 cm^{-1}. We assign the broad band observed in the $Fe^+(CO_2)_2$ spectrum to these sextet states. Notably, in the spectrum of $Fe^+(CO_2)_2Ar$, the broad band disappears entirely leaving only a very sharp band blue-shifted by 40 cm^{-1}. In addition to the spectral advantages normally observed for rare gas atom tagging, we suggest that the disappearance of the broad band is also related to the favored ground state of $Fe^+(CO_2)_2Ar$. Because additional ligands disfavor the sextet states of iron cation complexes over quartet states, the addition of an Ar atom to the $Fe^+(CO_2)_2$ molecule probably only occurs efficiently for $Fe^+(CO_2)_2$ complexes in their quartet ground state. Thus, no $Fe^+(CO_2)_2Ar$ complexes in a sextet excited state are present, thereby removing the broad band observed near 2349 cm^{-1} for $Fe^+(CO_2)_2$.

The spectra of $Fe^+(CO_2)_3$ and $Fe^+(CO_2)_3Ar$ exhibit strong bands blue-shifted by 27 cm^{-1} from free CO_2. The $Fe^+(CO_2)_3$ spectrum also has a weak band (shifted by about 50 cm^{-1}) and the $Fe^+(CO_2)_3Ar$ spectrum shows a weak band to the red of the main peak (shifted by about 20 cm^{-1} from free CO_2). Gregoire and Duncan tentatively assign this spectrum to a trigonal planar geometry, with the weak bands representing minor isomers in the beam. As noted above, our calculations

of $Fe^+(CO_2)_3$ find that the quartet ground state is distorted from trigonal planar symmetry because of residual 4s−3dσ hybridization. Therefore, there are three IR active bands predicted to lie 15, 27, and 48 cm^{-1} to the blue of the free CO_2 band, with relative IR intensities of 0.8, 1.0, and 0.0 (where the latter band is nearly but not quite forbidden). In contrast, the spectrum predicted for the $^6A'$ state has two strong bands located near the free CO_2 band (shifts of −8 and 6 cm^{-1}) with a weak band blue-shifted by 40 cm^{-1}. Clearly, the predictions for the $^4A'$ state agree reasonably well with the observed spectrum.

$Fe^+(CO_2)_4$ and $Fe^+(CO_2)_4Ar$ both exhibit a sharp strong band blue-shifted by 18 cm^{-1} from free CO_2. A weak band at about 30 cm^{-1} is also observed in the $Fe^+(CO_2)_4$ spectrum. Gregoire and Duncan concluded that $Fe^+(CO_2)_4$ is likely to have tetrahedral structure rather than a square planar geometry, on the basis of the propensity for adding Ar atoms. Our calculations of the $Fe^+(CO_2)_4$ complex find it has a distorted tetrahedral geometry, with three bands that are strongly IR active having shifts of 13, 16, and 16 cm^{-1}, and a fourth band that is nearly IR inactive at 49 cm^{-1} above free CO_2. These features are consistent with the observed spectrum. Predictions for the near square planar doublet state of $Fe^+(CO_2)_4$ find two strong bands at about 24 cm^{-1} above free CO_2 and two nearly forbidden bands with shifts of 12 and 59 cm^{-1}, in poorer agreement with the observed spectrum.

For the largest complex studied here, $Fe^+(CO_2)_5$, Gregoire and Duncan observe a main band shifted to the blue by 17 cm^{-1} from the value for free CO_2. In addition, there is a less intense band (about 1/4 the intensity of the main band) at about 2385 cm^{-1}, a shift of 36 cm^{-1}. Another band of medium intensity is found at the unperturbed frequency of 2349 cm^{-1} and attributed to ligands attached in the second solvent shell. Our calculations find that both the quartet and doublet states have predicted spectra reasonably consistent with this although the quartet state gives the closest agreement with intense bands predicted at shifts of 16 and 17 cm^{-1}, and weak bands at 12 and 49 cm^{-1}. In these complexes, the ligands that bind in much different modes (side-on for the quartet state and C−C coupling for the doublet) have their asymmetric stretch frequencies shifted strongly to the red (by hundreds of wavenumbers), outside the range studied spectroscopically.

5. Conclusion

Kinetic energy dependent collision-induced dissociation in a guided ion beam tandem mass spectrometer is used to determine the absolute bond energies of $Fe^+(CO_2)_n$ for $n = 1-5$. Effects of multiple collisions, internal energies of the complexes, reactant translational energy distributions, and dissociation lifetimes are all considered in the analysis of the experiments. Our experimental results show a strong BDE for $n = 2$ and a weak BDE for $n = 3$. Notably, the BDEs for the fourth and fifth ligand are stronger than that of the third.

A strong second ligand BDE can be explained by 4s−3dσ hybridization, which removes electron density along the bonding axis for two ligands at 180°. In addition, the cost of exciting Fe^+ ion from sextet to quartet state, which makes the hybridization more effective by localizing two electrons away from the σ axis, is shared as well as the cost of hybridization. Calculations indicate that loss of such hybridization is partially retained in $Fe^+(CO_2)_3$, which results in a constrained geometry with ligand−ligand steric interactions and a weak BDE for the third CO_2 ligand. Relatively strong BDEs for the fourth and fifth CO_2 ligands follows the trend in BDEs previously found for π-accepting ligands (such as CO, N_2, and H_2), even though calculations indicate that the π interactions of CO_2 with first row transition metal ions are weak.[9] In general, the BDE of CO_2 is weaker than CO and stronger than N_2.

Although the trends of the theoretical BDEs at the BHandH and B3LHYP levels of theory roughly follow those of the experiment, the agreement of absolute BDEs between theory and experiment is unsatisfying especially for $n = 4$ and 5. These floppy molecules are particularly challenging for ab initio calculations and more sophisticated theory (perhaps CASSCF) is required to resolve these discrepancies. However, the theory does provide an adequate prediction of the infrared spectra of these complexes in the region of the asymmetric CO_2 stretch and provides new insight into the observations of Gregoire and Duncan.[11]

Acknowledgment. This work is supported by the National Science Foundation, Grants CHE-0135517 and CHE-0451477.

Supporting Information Available: Table 1S, theoretical energies, zero point energies, rotational constants, and vibrational frequencies of $Fe^+(CO_2)_n$ complexes, and Table 2S, geometrical parameters of the $Fe^+(CO_2)_n$ complexes. This material is available free of charge via the Internet at http://pubs.acs.org.

References and Notes

(1) Behr, A. *Carbon Dioxide Activation by Metal Complexes*; VCH: New York, 1998.
(2) Palmer, D. A.; Eldik, R. V. *Chem. Rev.* **1983**, *96*, 651.
(3) Gibson, D. H. *Chem. Rev.* **1996**, *96*, 2063.
(4) Solymosi, F. J. *Mol. Catal.* **1991**, *65*, 337.
(5) Louie, J.; Gibby, J. E.; Farnworth, M. V.; Tekavec, T. N. *J. Am. Chem. Soc.* **2002**, *124*, 15188.
(6) Schwarz, J.; Heinemann, C.; Schwarz, H. *J. Phys. Chem.* **1995**, *99*, 11405.
(7) Dieterle, M.; Harvey, J. N.; Heinemann, C.; Schwarz, J.; Schröder, D.; Schwarz, H. *Chem. Phys. Lett.* **1997**, *277*, 399.
(8) Tjelta, B. L.; Walter, D.; Armentrout, P. B. *Int. J. Mass Spectrom. Ion Processes* **2001**, *204*, 7.
(9) Sodupe, M.; Branchadell, V.; Rosi, M.; Bauschlicher, C. W. *J. Phys. Chem. A.* **1997**, *101*, 7854.
(10) Fan, H. J.; Liu, C. W. *Chem. Phys. Lett.* **1999**, *300*, 351.
(11) Gregoire, G.; Duncan, M. A. *J. Chem. Phys.* **2002**, *117*, 2120.
(12) Schultz, R. H.; Crellin, K. C.; Armentrout, P. B. *J. Am. Chem. Soc.* **1991**, *113*, 8590.
(13) Schultz, R. H.; Armentrout, P. B. *J. Phys. Chem.* **1993**, *97*, 596.
(14) Tjelta, B. L.; Armentrout, P. B. *J. Phys. Chem.* **1997**, *101*, 2064.
(15) Walter, D.; Armentrout, P. B. *J. Am. Chem. Soc.* **1998**, *120*, 3176.
(16) Bushnell, J. E.; Kemper, P. R.; Bowers, M. T. *J. Chem. Phys.* **1995**, *99*, 15602.
(17) Rodgers, M. T.; Armentrout, P. B. *Mass Spectrom. Rev.* **2000**, *19*, 215.
(18) Ervin, K. M.; Armentrout, P. B. *J. Chem. Phys.* **1985**, *83*, 166.
(19) Schultz, R. H.; Armentrout, P. B. *Int. J. Mass Spectrom. Ion Processes* **1991**, *107*, 29.
(20) Muntean, F.; Armentrout, P. B. *J. Chem. Phys.* **2001**, *115*, 1213.
(21) Dalleska, N. F.; Honma, K.; Sunderlin, L. S.; Armentrout, P. B. *J. Am. Chem. Soc.* **1994**, *116*, 3519.
(22) Schultz, R. H.; Armentrout, P. B. *J. Chem. Phys.* **1992**, *96*, 1046.
(23) Khan, F. A.; Clemmer, D. E.; Schultz, R. H.; Armentrout, P. B. *J. Phys. Chem.* **1993**, *97*, 7978.
(24) Rodgers, M. T.; Armentrout, P. B. *J. Phys. Chem. A* **1997**, *101*, 1238.
(25) Gerlich, D. In *State-Selected and State-to-State Ion−molecule Reaction Dynamics, Part 1, Experiment*, Ng, C. Y.; Baer, M., Eds.; Advances in Chemical Physics Series LXXXII; Wiley: New York, 1992; p 1.
(26) Aristov, N.; Armentrout, P. B. *J. Phys. Chem.* **1986**, *90*, 5135.
(27) Corliss, C.; Sugar, J. *J. Phys. Chem. Ref. Data, Suppl. 2* **1985**, *14*, 1.
(28) Wachters, A. J. H. *J. Chem. Phys.* **1970**, *52*, 1033.
(29) Hay, P. J. *J. Chem. Phys.* **1977**, *66*, 4377.
(30) Almlof, J.; Taylor, P. R. *J. Chem. Phys.* **1987**, *86*, 4070.
(31) Frisch, M. J.; Trucks, G. W.; Schlegel, H. B.; Scuseria, G. E.; Robb, M. A.; Cheeseman, J. R.; Zakrzewski, V. G.; Montgomery, J. A.; Stratmann, R. E.; Burant, J. C.; Dapprich, S.; Millam, J. M.; Daniels, A. D.; Kudin, K. N.; Strain, M. C.; Farkas, O.; Tomasi, J.; Barone, V.; Cossi, M.; Cammi,

R.; Mennucci, B.; Pomelli, C.; Adamo, C.; Clifford, S.; Ochterski, J.; Petersson, G. A.; Ayala, P. Y.; Cui, Q.; Morokuma, K.; Malick, D. K.; Rabuck, A. D.; Raghavachari, K.; Foresman, J. B.; Cioslowski, J.; Ortiz, J. V.; Stefanov, B. B.; Liu, G.; Liashenko, A.; Piskorz, P.; Komaromi, I.; Gomperts, R.; Martin, R. L.; Fox, D. J.; Keith, T.; Al-Laham, M. A.; Peng, C. Y.; Nanayakkara, A.; Gonzalez, C.; Challacombe, M.; Gill, P. M. W.; Johnson, B. G.; Chen, W.; Wong, M. W.; Andres, J. L.; Head-Gordon, M.; Replogle, E. S.; Pople, J. A. Gaussian, Inc.: Pittsburgh, PA, 1998.

(32) Herzberg, G. *Molecular Spectra and Molecular Structure*; Van Nostrand Reinhold: New York, 1966; Vol. III.

(33) Rodgers, M. T.; Ervin, K. M.; Armentrout, P. B. *J. Chem. Phys.* **1997**, *106*, 4499.

(34) Beyer, T. S.; Swinehart, D. F. *Comm. Assoc. Comput. Machinery* **1973**, *16*, 379.

(35) Stein, S. E.; Rabinovitch, B. S. *J. Chem. Phys.* **1973**, *58*, 2438.

(36) Stein, S. E.; Rabinovitch, B. S. *Chem. Phys. Lett.* **1977**, *49*, 183.

(37) Gilbert, R. G.; Smith, S. C. *Theory of Unimolecular and Recombination Reactions*; Blackwell Scientific Publications: Oxford, U.K., 1990.

(38) Marcus, R. A.; Rice, O. K. *J. Phys. Colloid Chem.* **1951**, *55*, 894.

(39) Marcus, R. A. *J. Chem. Phys.* **1952**, *20*, 359.

(40) Rosenstock, H. M.; Wallenstein, M. B.; Wahrhaftig, A. L.; Eyring, H. *Proc. Natl. Acad. Sci. U.S.A.* **1952**, *38*, 667.

(41) Hales, D. A.; Lian, L.; Armentrout, P. B. *Int. J. Mass Spectrom. Ion Processes* **1990**, *102*, 269.

(42) Waage, E. V.; Rabinovitch, B. S. *Chem. Rev.* **1970**, *70*, 377.

(43) Boo, B. H.; Armentrout, P. B. *J. Am. Chem. Soc.* **1987**, *109*, 3459.

(44) Ervin, K. M.; Armentrout, P. B. *J. Phys. Chem.* **1984**, *88*, 5454.

(45) Armentrout, P. B. In *Structure/Reactivity and Thermochemistry of Ions*; Ausloos, P., Lias, S. G., Eds.; Reidel: Dordrecht, The Netherlands, 1987; p 97.

(46) Armentrout, P. B. In *Advances in Gas-phase Ion Chemistry*; Adams, N. G., Babcock, L. M., Eds.; JAI: Greenwich, U.K., 1992; Vol. 1, p 83.

(47) Armentrout, P. B.; Simons, J. *J. Am. Chem. Soc.* **1992**, *114*, 8627.

(48) Andersen, A.; Muntean, F.; Walter, D.; Rue, C.; Armentrout, P. B. *J. Phys. Chem. A* **2000**, *104*, 692.

(49) Sodupe, M.; Bauschlicher, C. W., Jr.; Partridge, H. *Chem. Phys. Lett.* **1992**, *192*, 185.

(50) Gillespie, R. J. *J. Chem. Educ.* **1963**, *40*, 295.

(51) Ricca, A.; Bauschlicher, C. W., Jr. *J. Phys. Chem.* **1994**, *98*, 12899.

(52) Ricca, A.; Bauschlicher, C. W., Jr. *J. Phys. Chem.* **1995**, *99*, 9003.

(53) Brinckman, N. R.; Schaefer, H. F. Unpublished work cited in ref 11.